Struct Multidisc Optim (2006) 31: 60–75
DOI 10.1007/s00158-005-0555-8

RESEARCH PAPER

Mahmoud I. Hussein · Karim Hamza · Gregory M. Hulbert · Richard A. Scott · Kazuhiro Saitou

Multiobjective evolutionary optimization of periodic layered materials for desired wave dispersion characteristics

Received: 28 November 2004 / Revised manuscript received: 20 April 2005 / Published online: 27 October 2005

Abstract An important dispersion-related characteristic of wave propagation through periodic materials is the existence of frequency bands. A medium effectively attenuates all incident waves within stopbands and allows propagation within passbands. The widths and locations of these bands in the frequency domain depend on the layout of contrasting materials and the ratio of their properties. Using a multiobjective genetic algorithm, the topologies of one-dimensional periodic unit cells are designed for target frequency band structures characterizing longitudinal wave motion. The decision variables are the number of layers in the unit cell and the thickness of each layer. Binary and mixed formulations are developed for the treatment of the optimization problems. Designs are generated for the following novel objectives: (1) maximum attenuation of time harmonic waves, (2) maximum isolation of general broadband pulses, and (3) filtering signals at predetermined frequency windows. The saturation of performance with the number of unit-cell layers is shown for the first two cases. In the filtering application, the trade-off between the simultaneous realization of passband and stopband targets is analyzed. It is shown that it is more difficult to design for passbands than it is to design for stopbands. The design approach presented has potential use in the development of vibration and shock isolation structures, sound isolation pads/partitions, and multiple band frequency filters, among other applications.

Keywords Periodic materials · Phononic and photonic crystals · Wave dispersion · Band gap · Stopband · Passband · Topology optimization · Multiobjective genetic algorithms · Vibration and shock isolation

Mahmoud I. Hussein (✉) · Karim Hamza · Gregory M. Hulbert · Richard A. Scott · Kazuhiro Saitou
Department of Mechanical Engineering,
The University of Michigan,
2350 Hayward Street, 2250 GG Brown Building,
Ann Arbor, MI, 48109, USA
e-mail: husseinm@engin.umich.edu
e-mail: khamza@engin.umich.edu
e-mail: hulbert@engin.umich.edu
e-mail: car@engin.umich.edu
e-mail: kazu@engin.umich.edu

1 Introduction

Wave propagation in heterogeneous media is dispersive, i.e., a wave decomposes into multiple waves with different frequencies. In media with periodic heterogeneity, there are ranges of frequencies, known as *stopbands* or *band gaps*, over which all incident waves are effectively attenuated. This attenuation phenomenon is attributed to a mechanism of destructive interferences within the scattered wave field. In complementary frequency bands, *passbands*, constructive interferences dominate and waves effectively propagate through the medium. This frequency-banded dynamic response has triggered much interest in periodic materials, especially since these materials have practical applications across multiple disciplines (e.g., photonic crystals are used to control the propagation of electromagnetic waves, and phononic materials, or sonic crystals, are used to control the motion of acoustic and elastic waves). The reader is referred to an extensive review article on this broad field (Kushwaha 1996). Of increasing interest is the design of periodic materials for desired wave dispersion characteristics, which, in turn, provides a means for passive control of the wave fields in the materials in accordance to the requirements of the given application. A review article on the inverse problem has recently been published (Burger et al. 2004).

From a practical perspective, it has been shown that as long as a sufficient number of cells are available (usually around three to four are required), bounded structures formed from periodic materials can exhibit similar wave attenuation characteristics to those of the periodic materials (e.g., Day et al. 1994; Cao and Qi 1995; Jensen 2003; Hussein et al. 2003, 2004b, 2005; Hussein 2004).

By controlling the materials layout and the ratio of their properties within a unit cell, a periodic composite could be designed to have a desired frequency band structure (the size and location of stopbands). In this work, bimaterial layered (one-dimensional) composites are considered where the unit cell consists of sublayers of alternating material types with different thicknesses. The frequency band structure can therefore be controlled by varying the configuration of the layers. Three case studies are considered:

Case I Creation of a stopband for maximized wave atten-

uation at a specified frequency

Case II Maximization of the percentage of stopbands within a specified large frequency range for minimum wave transmissibility

Case III Creation of multiple stopbands/passbands at specified frequency ranges

The designed materials could be used for isolating vibrations induced by single (case I) or multiple (case III) harmonic excitation. Material designs for case II could find application for shock isolation (defining a shock load as one that consists of a transient broadband pulse) and sound isolation in which the frequency spectrum is typically broad.

In all the considered cases, the decision variables are (1) the number of layers in the unit cell and (2) the thickness of each of the layers. The maximum number of unit-cell layers and the range of admissible layer thicknesses are important quantities from both the dynamic performance and practical points of view. Increasing these quantities provides more precise control of the frequency band structure, but it entails higher manufacturing costs. For practical considerations, there are limits (constraints) on (1) the minimum layer thickness and (2) the total cell length (the cell length is conveniently assigned with the value of unity).

Cases I and II are posed as multiobjective optimization problems where the number of cell layers and their thicknesses are optimized for maximum wave attenuation capacity with minimum number of layers. For case II, an additional study is carried out where the frequency content of the excitation load that is to be isolated is incorporated as a weighting function. This forces the locations of the generated band gaps to be biased towards the high-magnitude frequencies of the excitation load. Two formulations of the decision variables are developed, each with its own advantages (as will emerge). The first is a mixed-integer programming, where the number of layers is represented by an integer variable, and the layer thicknesses are represented as continuous variables. The second formulation is a zero–one integer programming, where the unit cell is divided into a fixed number of imaginary divisions, and the material type of each division is represented by the binary variables. In this manner, the binary variables control both the number and the thicknesses of the actual layers. Solutions to both formulations are attempted using an evolutionary optimization technique. A multiobjective genetic algorithm, namely, the Nondominated Sorting Genetic Algorithm (NSGA-II; Deb et al. 2000, Deb 2001), is employed. NSGA-II is a heuristic algorithm capable of efficiently generating quasi-Pareto optimal (noninferior) solutions.

For case III, only the binary formulation is followed, and the two previous competing objectives are replaced with the ones that are related solely to dynamic performance (namely, achievement of attenuation at specified frequency ranges and propagation at complementary frequency ranges). The multiobjective genetic algorithm described above is also used for case III.

A similar design problem to that of case I has been pursued in the contexts of electromagnetic (Cox and Dobson 1999, 2000) and elastodynamic (Sigmund and Jensen 2003) wave propagation. In all these studies, two-dimensional periodic unit cells were optimized to produce a band gap (between two selected branches) with a maximum width and centered at a given frequency or at a minimum frequency. Local search optimization techniques were used. However, optimization problems on frequency band structures tend to be highly multimodal, and therefore, it is possible for a local search to converge to local optima. In this paper, the technique of genetic algorithms is chosen because it has the advantage that it simultaneously evolves multiple designs and eventually converges to near-global optimality.

In a previous work (Hussein et al. 2002) dealing with longitudinal wave propagation in layered periodic materials, cases I and II were pursued (as single-objective optimization problems). For a given maximum limit on the number of layers, the optimal design for each case was found by exhaustively searching over all possible cell configurations under the restriction that layers only could have thicknesses that are multiples of a minimum size. While the exhaustive search guarantees finding a global optimum, it is prohibitively expensive because the number of possible combinations of layer thicknesses increases exponentially with the number of layers. The adoption of genetic algorithms in this study efficiently extends the design space and therefore allows for better designs to be realized (preliminary results are presented in Hussein et al. 2004a).

The new features of the present study are summarized as follows: (1) multiobjective optimization where a dynamic performance measure trades off with a manufacturing cost-related objective (cases I and II) or with another dynamic performance objective (case III); (2) employment of an objective function for the dynamic performance in case I that focuses solely on the attenuation strength as opposed to the width and location of the band gap; (3) design of band-gap materials for shock isolation (case II); (4) weighted band structure optimization where the frequency content of the excitation is incorporated in the formulation (second part of case II); (5) design for multiple stopbands and passbands, i.e., high-order filters (case III); and (6) development, and comparison, of a mixed formulation and a binary formulation for optimizing layered band-gap materials.

The rest of the paper is organized as follows. Section 2.1 describes the mathematical formulation of a transfer matrix

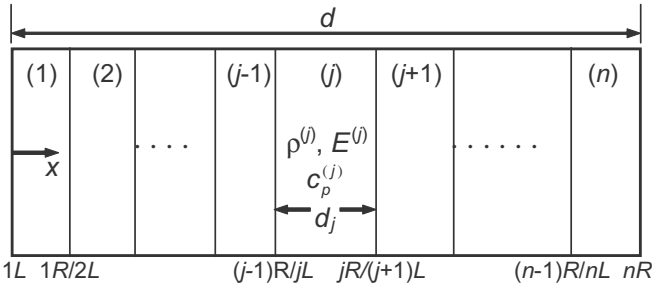

Fig. 1 Unit cell consisting of *n* layers (layer number indicated in *parentheses*)

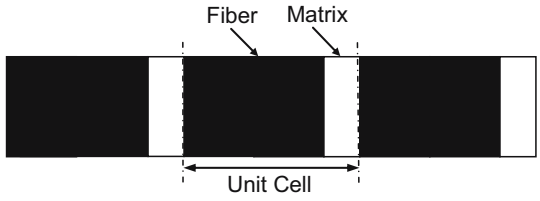

Fig. 2 Infinite layered medium (three unit cells shown)

method for computing frequency spectra (i.e., frequency vs wave number dispersion curves) for linear elastic periodic materials, and in Section 2.2, the dispersive response of a corresponding finite periodic structure (undamped and damped) is considered. In Section 3, the two formulations of the cell design problem are presented along with a description of the employed multiobjective genetic algorithm and the implementation techniques. Section 4 presents the description and results of the three case studies. A summary is provided and conclusions are drawn in Section 5.

2 Dispersive wave motion in periodic layered materials and structures

2.1 Unit-cell analysis

Consider a general multilayered medium (as depicted in Fig. 1) where an arbitrary layer j is shown to be positioned between an adjacent layer $j-1$ at its left and an adjacent layer $j+1$ at its right. The interface between the layers is assumed to be ideal. The jth layer has thickness d_j, density $\rho^{(j)}$, Young's modulus $E^{(j)}$, and longitudinal velocity $c_{\mathrm{p}}^{(j)} = \sqrt{E^{(j)}/\rho^{(j)}}$, respectively. For this one-dimensional model, the elastodynamic response is determined using Floquet's (1883) theorem and the transfer matrix method (Thomson 1950). Combining these tools provides an exact elasticity solution for the frequency spectrum (Esquivel-Sirvent and Cocoletzi 1994; Shen and Cao 2000; Hussein et al. 2005).

The governing equation for longitudinal wave propagation in the x direction in the jth layer is:

$$\frac{\partial^2 u(x,t)}{\partial t^2} = (c_{\mathrm{p}}^{(j)}(x))^2 \frac{\partial^2 u(x,t)}{\partial x^2}, \tag{1}$$

where u is the displacement field and t denotes time. The boundary conditions that must be satisfied at the layer interfaces are (1) the continuity of the displacement u and (2) the continuity of the traction (stress) σ. The solution of Eq. 1 in the jth layer can be written as a superposition of forward and backward traveling waves with harmonic time dependence:

$$u(x,t) = \left[A_+^{(j)} \mathrm{e}^{ik_{\mathrm{p}}^{(j)}x} + A_-^{(j)} \mathrm{e}^{-ik_{\mathrm{p}}^{(j)}x}\right] \times \mathrm{e}^{-i\omega t}, \tag{2}$$

where $i = \sqrt{-1}$, $k_{\mathrm{p}}^{(j)} = \omega/c_{\mathrm{p}}^{(j)}$, and ω is the temporal frequency. The stress component is given by

$$\sigma(x,t) = E^{(j)}(x) \frac{\partial u(x,t)}{\partial x}. \tag{3}$$

Let $x^{j\mathrm{L}}$ and $x^{j\mathrm{R}}$ denote the position along the x-axis of the left and right boundaries of layer j, respectively. From Eqs. 2 and 3, and using the relation $x^{j\mathrm{R}} = x^{j\mathrm{L}} + d_j$, the values of the

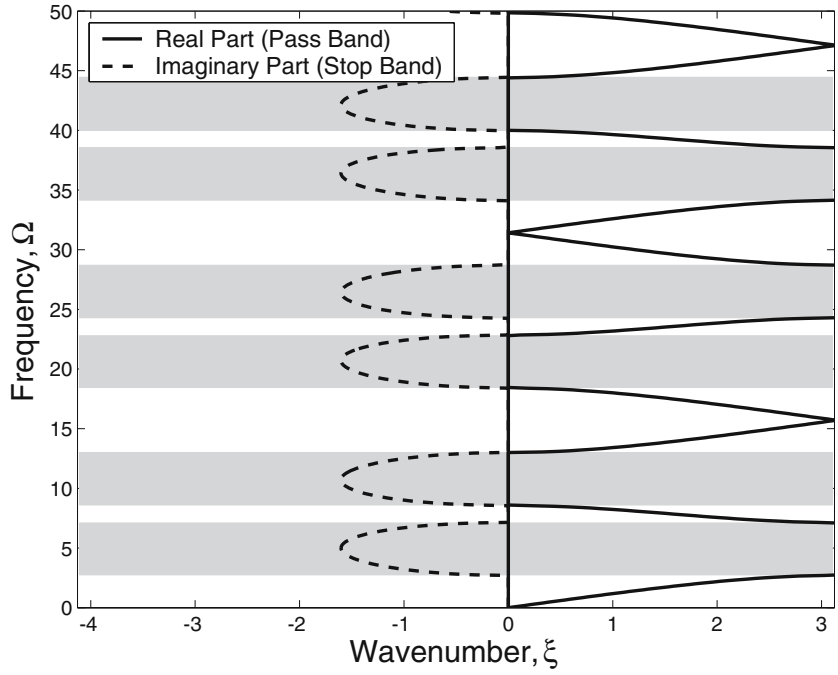

Fig. 3 Dispersion curves for longitudinal wave propagation normal to the layers in the infinite periodic structure shown in Fig. 2 (stop bands *shaded in gray*)

displacement u and stress σ at $x^{j\mathrm{L}}$ are related to those at $x^{j\mathrm{R}}$. Through a *transfer matrix* $\mathbf{T}_j$, this mapping can be repeated recursively to relate the displacements and the stresses across several layers. For the n-layered system shown in Fig. 1, a cumulative transfer matrix $\mathbf{T} = \mathbf{T}_n\mathbf{T}_{n-1}\cdots\mathbf{T}_1$ is constructed:

$$\begin{bmatrix} u_1 \\ \sigma \end{bmatrix}_{x^{n\mathrm{R}}} = \mathbf{T}\begin{bmatrix} u \\ \sigma \end{bmatrix}_{x^{1\mathrm{L}}}. \tag{4}$$

For an infinite periodic layered medium consisting of repeated unit cells, each consisting of n layers and has width $d = d_1 + d_2 + \cdots + d_n$, Floquet's theorem is used to relate the time harmonic response at a given cell to that at an adjacent cell:

$$\begin{bmatrix} u \\ \sigma \end{bmatrix}_{x+d} = \mathrm{e}^{ikd}\begin{bmatrix} u \\ \sigma \end{bmatrix}_{x}, \tag{5}$$

where k is a wave number corresponding to wave motion in the periodic medium. Coupling Eq. 4 with Eq. 5 results in the eigenvalue problem:

$$[\mathbf{T} - \mathbf{I}\mathrm{e}^{ikd}]\begin{bmatrix} u \\ \sigma \end{bmatrix}_{x^{1\mathrm{L}}} = 0, \tag{6}$$

which is solved for the dispersion curves (ω vs k). Furthermore, the time-dependent displacement mode shapes can be obtained using Eqs. 2, 4, and 5. A detailed description of the above procedure as well as an algorithm for computing the mode shapes has been presented previously (Hussein et al. 2005).

For the purpose of demonstration, consider the time harmonic wave propagation in a periodic layered medium with an arbitrarily chosen unit-cell design, as shown in Fig. 2. The unit cell is composed of two parallel layers of stiff (fiber) and compliant (matrix) materials. Using 'f' and 'm' subscripts to denote fiber and matrix, respectively, the dimensions are d_f/d=0.8. The ratios of the material properties are $\rho_\mathrm{f}/\rho_\mathrm{m}$=3 and $E_\mathrm{f}/E_\mathrm{m}$=12. It is should be noted that the dispersion characteristics are dependent on the ratios of layer geometries and material properties and not on their absolute values.

The dispersion curves for longitudinal waves propagating in the direction normal to the layering are computed and plotted in Fig. 3. The nondimensional frequency $\Omega = \omega d \Big/ \sqrt{E_\mathrm{m}/\rho_\mathrm{m}}$ and the nondimensional wave number $\xi = \xi_\mathrm{real} + i\xi_\mathrm{imag} = k \times d$ define the ordinate and abscissa, respectively. The solid lines represent the real part of the dispersion relation, and these appear as multiple branches of passband modes of wave propagation. The dashed lines represent the imaginary part of the dispersion relation, and these too appear as multiple branches, but of stopband modes. At passband frequencies, waves are "allowed" to effectively propagate across the medium. At stopband frequencies, incident waves are localized and attenuated in space, thus "forbidding" the effective transmission of energy across the layers.

The model and analysis presented above could be generalized to incorporate transverse wave motion as well as wave propagation parallel (as opposed to normal) to the layering. However, the same ideas hold with regards to the notion of designing periodic layered materials for desired dispersion characteristics. Hence, for the rest of this paper, the attention is focused on longitudinal wave propagation in the direction normal to the layering.

2.2 Dispersion in a finite periodic structure

For a periodic material's banded frequency characteristics to have practical significance, it is important that a finite (i.e., bounded) structure formed from this material exhibits similar wave attenuation characteristics. It has been shown that a minimum number of cells, e.g., three to four cells, are necessary for the response of a finite periodic structure to exhibit the same frequency bands as the constituent periodic material (Hussein et al. 2005). Such congruence of response is briefly demonstrated in this section through an example. Furthermore, viscous damping in a bounded periodic structure is considered to examine its effects.

As a demonstrative case study, the five-cell long structure (of length L=5) shown in Fig. 4 is considered (5 cells are included to be in the conservative side). The unit cell from which this structure is formed is the same as shown in Fig. 2. The stopbands of that unit cell are the horizontal bands shaded in Fig. 3. The structure is restrained from motion at the right end and is subjected to a prescribed harmonic force at the left end of the form

$$f_\mathrm{ext}(x,t) = F(x,\omega^*)\mathrm{e}^{i\omega^* t}, \tag{7}$$

where F is a complex coefficient and ω^* is the frequency of an applied harmonic force. A forced response frequency sweep (with a sampling step of $\Delta\Omega^* = 0.1$, where $\Omega^* = \omega^*\mathrm{d}\Big/\sqrt{\mathrm{E_m}/\rho_\mathrm{m}}$ is carried out to cover the entire range, $0 \le \Omega^* \le 50$, considered in Section 2.1. To incorporate the above forcing as well as viscous damping, the governing equation of motion is generalized to

$$\rho^{(j)}u_{,tt} + D^{(j)}u_{,t} - E^{(j)}u_{,xx} = f_\mathrm{ext}(x,t), \tag{8}$$

where $D^{(j)}$ is a damping coefficient associated with the jth layer. Superscripts $(\cdot)_{,x}$ and $(\cdot)_{,t}$ denote differentiation with

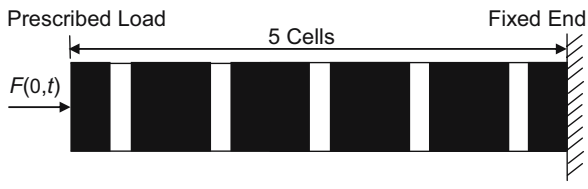

Fig. 4 Finite periodic structure consisting of five cells (*black and white colors* represent fiber and matrix, respectively). The structure has a fixed boundary condition at the right end. At the left end, a prescribed harmonic force is applied

respect to position and time, respectively. For simplicity, proportional material damping is considered (as commonly assumed in structural dynamics) and has the form

$$D^{(j)} = \beta\rho^{(j)} + \alpha E^{(j)}, \tag{9}$$

where β and α are parameters.

A standard finite element method is used to solve the above problem for two cases: (1) undamped and (2) damped with β=0.25 and α=0. The model consists of 600 piecewise linear elements, with lengths following the condition $h_{\mathrm{f}}^{\mathrm{e}} = 2h_{\mathrm{m}}^{\mathrm{e}}$, where h^{e} is the element size. The maximum displacement values within the fifth cell (i.e., at the receiving end of the structure) are plotted as a function of Ω^* in Fig. 5. All displacement values are normalized with respect to the static deflection of an equivalent homogenous structure, defined as

$$\delta = 5Fd/E_{\mathrm{avg}}, \tag{10}$$

where

$$E_{\mathrm{avg}} = \left(r_{\mathrm{f}}\frac{1}{E_{\mathrm{f}}} + r_{\mathrm{m}}\frac{1}{E_{\mathrm{m}}}\right)^{-1}, \tag{11}$$

and where r_{f} and r_{m} denote the fraction of stiff and compliant materials, respectively. The constituent unit-cell stopband frequency ranges are the vertical bands shaded in the figure. These are identical to the horizontally shaded stopbands in Fig. 3. It is clear that the dynamic behavior of both the undamped and damped finite periodic structures conform to the periodic material's frequency bands—and since as many as five unit cells are available, the attenuation at stopband frequencies is significant as desired. The damping suppresses the passband resonant modes and appears to have no effect on the stopband response. These results affirm that the frequency-banded characteristics of a unit cell matches with that of a corresponding finite, fully periodic structure, including a viscously damped structure. Hence, the process of unit-cell design (the focus of the rest of the paper) is sufficient for the design of finite periodic structures for both the undamped and damped cases.

3 Multiobjective genetic algorithm for unit-cell design

3.1 Cell design problem formulations: mixed and binary

Varying the number of layers of alternating materials and their thicknesses allows for "shaping" the frequency spectrum of the periodic medium. With this capability, a design can be generated with a desired distribution of stopbands and passbands to achieve a target dynamic performance. The details of performance measures are given in Section 4. Recall that the number of cell layers is n, and let the thicknesses be expressed in vector form, i.e., $\mathbf{d} = (d_1, d_2, \ldots, d_n)$. Since the unit cell is periodic, it is assumed, without loss of generality, that the first layer in the unit cell is always a fiber and that n is an even number. Using the integer variable n and the continuous variable $\mathbf{d}$, the problem can be formulated as a mixed-integer programming, which shall be referred to as the *mixed formulation*:

$$\text{Minimize} \quad f_1 = \mathrm{Pen}_1(n, \mathbf{d}),\ f_2 = \mathrm{Pen}_2(n, \mathbf{d}), \tag{12}$$

$$\text{Subject to} \sum_{j=1}^{n} d_j = 1, \tag{13}$$

$$d_j \geq a \ \text{for} \ j = 1, 2, ..., n, \tag{14}$$

$$2 \leq n \leq n_{\max},\ n\ is\ an\ even\ number, \tag{15}$$

$$\mathbf{d} \in \mathbb{R}^n, n \in \mathbb{Z}, \tag{16}$$

where

f_1, f_2: performance and/or cost objective functions. A performance objective is defined as a penalty on the deviation of the wave attenuation capacity of the medium at a specified frequency (or frequency range) from a desired target. A cost objective is defined as a penalty on the estimated manufacturing cost (assumed to increase with the number of layers in the unit cell)

a: minimum thickness of a layer given as a fraction of unity.

$n_{\max}$: maximum number of layers.

It should be noted that the dimension of vector variable $\mathbf{d}$ depends on another variable n, which often causes a difficulty in optimization algorithms. The constraint on the total cell length is unity by construction. For the other constraints, it is assumed that a and $n_{\max}$ are defined by the manufacturing limitations.

Alternatively, the problem can be formulated in terms of a vector of binary variables $\mathbf{b}$=(b_1, b_2,..., b_l) (with a constant dimension l) by assuming that a unit cell is divided into l imaginary "divisions" or "slots," each of which can be filled with either fiber 'f' or matrix 'm' (Hussein et al. 2002):

$$b_i = \begin{cases} 0 \text{ if slot } i \text{ is filled with fiber 'f'} \\ 1 \text{ if slot } i \text{ is filled with matrix 'm'.} \end{cases} \tag{17}$$

Contiguous slots filled with the same material form a homogenous continuum and are regarded as one cell layer. With this description, the total number of layers is

$$n = \sum_{i=1}^{l-1} s_i + 1, \tag{18}$$

where $\boldsymbol{s}$=(s_1, ..., s_{l-1}), s_i=XOR(b_i, b_{i+1}). The thickness d_j of layer j can take only discrete values with a multiple of 1/l, which can be expressed as:

$$d_j = (q_j - q_{j-1}) \times \frac{1}{l}, \tag{19}$$

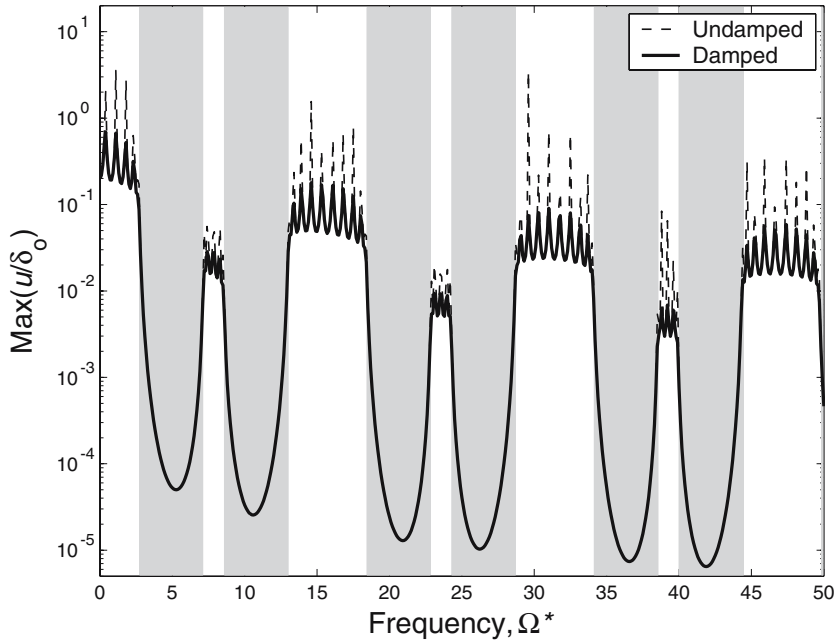

Fig. 5 Maximum displacement amplitude within fifth (rightmost) cell of structure shown in Fig. 4 vs frequency of excitation for undamped and damped cases. Stop bands corresponding to the periodic material's unit cell are *shaded in gray*

where $\boldsymbol{q}=(q_0, q_1, ..., q_n)$ are the indices of **s** with $s_i=1$, sorted in ascending order with $q_0=0$ and $q_n=l$. This formalism implies that $n=\dim(\mathbf{q})-1$. For example, if $l=10$ and $\mathbf{b}=(0,0,0,1,1,1,1,0,0,1)$, then $\mathbf{s}=(0,0,1,0,0,0,1,0,1)$ and $\mathbf{q}=(0,3,7,9,10)$, and hence $n=4$ and $\mathbf{d}=(0.3,0.4,0.2,0.1)$, starting with a fiber material for the first layer and alternating thereafter.

Using **b** as an independent design variable, the problem can now be formulated as zero–one integer programming, which shall be referred to as the *binary formulation*:

$$\text{Minimize: } \{f_1 = \text{Pen}_1(n, \mathbf{d}),\ \ f_2 = \text{Pen}_2(n, \mathbf{d})\}\,, \tag{20}$$

$$\text{Subject to: } n = \sum_{i=1}^{l-1} s_i + 1,\ s_i = \text{XOR}(b_i, b_{i+1}) \quad \text{for } i = 1, 2, \ldots, l-1, \tag{21}$$

$$d_j = (q_j - q_{j-1}) \times \tfrac{1}{l}, \quad q_j \text{ for } j = 0, \ldots, n, \text{ are as defined above,} \tag{22}$$

$$d_j \geq a \text{ for } j = 1, 2, \ldots, n, \tag{23}$$

$$2 \leq n \leq n_{\max},\ n \text{ is an even number,} \tag{24}$$

$$\mathbf{b} \in \{0, 1\}^l. \tag{25}$$

In the previous work (Hussein et al. 2002), the cell design problem was tackled using the binary formulation with $l=10$, and this small value allowed for an exhaustive search of 2^{10} alternatives. Since d_j can only be a multiple of $1/l$, the optimal cell design could be further improved with a larger l, which makes exhaustive search totally impractical. In this paper, a multiobjective genetic algorithm is chosen due to its efficiency for global optimization of discrete and/or continuous variables as described in the following section.

3.2 Multiobjective genetic algorithm

A multiobjective genetic algorithm employed in the following case studies is a variant of the NSGA-II (Deb et al. 2000, Deb 2001), whose steps are outlined as follows:

1. Create a population P of p random designs and evaluate their objective function values. Also, create empty sets Q and O.
2. Rank each design c in P according to the number of other designs dominating[1] c (rank 0 is Pareto optimal in P).
3. Store the designs with rank 0 into set O. Update O by removing any designs dominated by others in O. If the size of O reaches a prespecified number, remove the designs that are similar to others (based on Euclidian-distance crowding) to maintain the size, while promoting diversity.
4. Select two designs c_i and c_j in P with probability proportional to *p-rank*(c_i) and *p-rank*(c_j).
5. Crossover c_i and c_j to generate new design(s) with a certain probability.
6. Mutate the new design(s) with a certain probability.
7. Repair the new design(s) to maintain their feasibility and/or remove redundancy.

[1] For a vector-valued function $\boldsymbol{f}=(f_1, f_2, ..., f_n)$ to be minimized, a point $\boldsymbol{x}$ *dominates* $\boldsymbol{y}$ if $f_i(\boldsymbol{x}) \leq f_i(\boldsymbol{y})$ for *all* $i=1, 2, ..., n$, and $f_i(\boldsymbol{x}) < f_i(\boldsymbol{y})$ for at least *one* of $i=1, 2, ..., n$.

8. Evaluate the objective function values of the new design(s) and store in Q. If the size of Q is less than p, go to step 4.
9. Replace P with Q, empty Q, and increment the generation counter. If the generation counter has reached a prespecified number, terminate the process and return O. Otherwise, go to step 2.

Due to the differences in the design variables, the two formulations of the cell design problem require different implementations of crossover, mutation, and repair at steps 6, 7, and 8. The details of these implementations are explained in the following sections.

3.3 Implementation of the mixed formulation

For the mixed formulation, a design is represented as a pair $(n, \bar{\mathbf{d}})$, where $\bar{\mathbf{d}}$ is a vector of constant size $n_{\max}$ with $\bar{d}_i = d_i$ for i=1, 2, ..., n.

3.3.1 Crossover and mutation

The crossover operator produces one new design $(n', \bar{\mathbf{d}}')$ from two "parent" designs $(n_1, \bar{\mathbf{d}}_1)$ and $(n_2, \bar{\mathbf{d}}_2)$, implemented as a combination of arithmetic and heuristic crossovers (Michalewicz 1996):

$$n' = 2\lfloor (n_1 + 2\alpha(n_2 - n_1))/2 \rfloor \tag{26}$$

$$\bar{\mathbf{d}}' = \bar{\mathbf{d}}_1 + 2\alpha(\bar{\mathbf{d}}_2 - \bar{\mathbf{d}}_1) \tag{27}$$

Prior to crossover, the selected parents are reordered such that $(n_1, \bar{\mathbf{d}}_1)$ is the better design (not dominated by $(n_2, \bar{\mathbf{d}}_2)$). The variable α is a random number between 0 and 1 (uniformly distributed). The factor "2" in the second term in Eqs. 26 and 27 is due to combining the arithmetic and heuristic crossovers. If α<0.5, the new design is always one that stands "between" the parent designs (as in the case of arithmetic crossover), whereas if α>0.5, the new design is projected outwards in the direction of the better design (as in the case of heuristic crossover). These types of crossover are reported to function well with continuous variables (Michalewicz 1996); hence, it is applied to $\bar{\mathbf{d}}$ with a high probability.

Since there is no restriction on the crossover between chromosomes representing designs of different layer lengths, a situation may occur whereby $n_1 \neq n_2$. The crossover on the discrete variable n effectively changes the number of layers, which can invalidate the physical meaning of allele values on portions of $\bar{\mathbf{d}}$. This is analogous to mutation effects, and for that reason, the crossover on the number of layers is performed according to Eq. 26 with low probability. Otherwise, n' is taken as the maximum of n_1 and n_2.

Mutation is applied with a low probability to every variable in $(n', \bar{\mathbf{d}}')$ by randomly changing the variable values to some value within its allowed range (i.e., uniform mutation).

3.3.2 Repair

The repair operator for the mixed formulation performs the following steps:

- The value of n is set to its nearest even number between 2 and $n_{\max}$. Although the crossover in Eq. 26 automatically produces even numbers, this step is to adjust the effect of uniform mutation on n.
- The values of $\bar{d}_i$ for i>n (which are physically meaningless) are set to zero to remove chromosome redundancy (chromosomes having different allele values that represent the same physical design).
- A linear transformation is performed such that $\bar{d}'_1 + \bar{d}'_2 + \cdots + \bar{d}'_n = 1$ and $\bar{d}'_i \geq a$ for i=1, 2, ..., n.

3.4 Implementation of the binary formulation

For the binary formulation, a design is simply represented as binary vector $\mathbf{b}$.

3.4.1 Crossover and mutation

Classic multipoint crossover and bit-flip mutation (Goldberg 1989) are applied.

3.4.2 Repair

Since the design performance depends only on the unit cell number of layers, the layer thicknesses, and the layering sequence (i.e., which layer follows which, but not which layer starts first), a repair operator that effectively cuts the search space by a factor of 4 is implemented as follows:

- Left-rotation of the chromosome bits is performed until b_1=0 (first bit is zero) and b_l=1 (last bit is assigned the value of unity)

This repair operator automatically ensures that the number of layers is an even number greater than or equal to 2, but does not guarantee that the minimum layer thickness is $\geq a$. However, if the division thickness is chosen such that $1/l \geq a$ (as in all cases considered in this work), the constraint on the minimum layer thickness is intrinsically satisfied.

4 Case studies: cell designs for desired frequency spectra

4.1 Case I: creation of a stopband for maximized attenuation at a specified frequency

The aim in this case study is to design a unit cell consisting of 'f' and 'm' materials (same properties as in Section 2), which provides maximum stopband attenuation at a predetermined nondimensional frequency Ω^*. From a practical perspective, a finite structure composed of several cells of

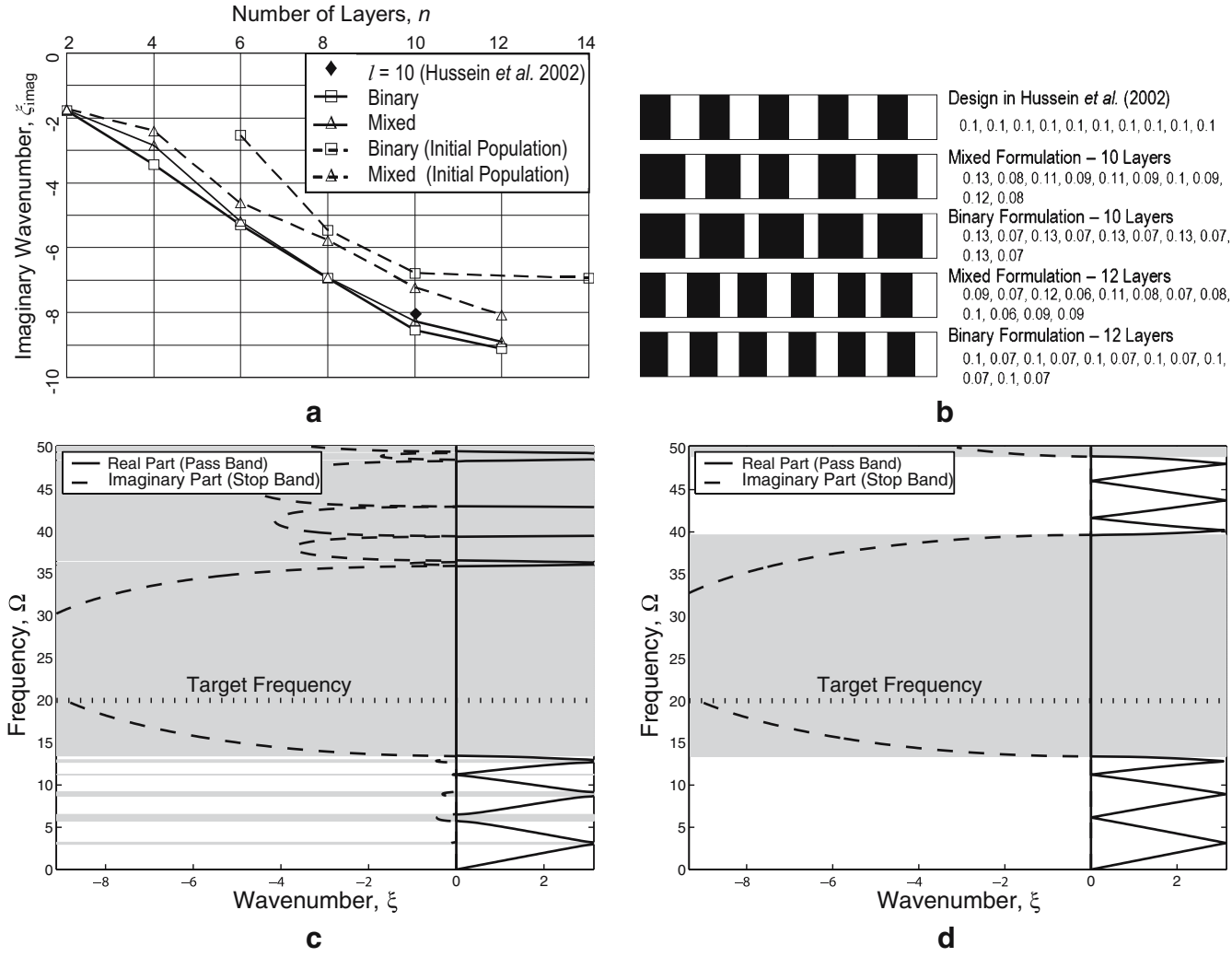

Fig. 6 Case I (maximization of stopband attenuation at $\Omega^*=20$): **a** Pareto diagram ($l=30$ for both mixed and binary formulations), **b** selected unit cell designs from the Pareto front. Frequency spectrum for twelve-layer design obtained by **c** the mixed formulation and **d** the binary formulation (stop bands *shaded in gray*)

such a design could be used to attenuate the propagation of a single harmonic wave resulting from an external excitation at a frequency ω^* (the size d of the cells and the properties of the 'm' material are also specified). It is known that the strength of spatial attenuation of an incident wave at a stopband frequency is exponentially related to the value of the corresponding imaginary wave number. On this basis, the value of the imaginary wave number (which is negative) at the predetermined frequency is taken as the performance objective function f_1 for the design problem:

$$\text{Minimize: } f_1 = \xi_{\text{imag}}(\Omega^*). \tag{28}$$

In contrast to objectives expressed in terms of band-gap size (like those chosen by Cox and Dobson 1999, 2000; Sigmund and Jensen 2003), the objective of Eq. 28 ensures that the performance credit is solely related to the strength of attenuation. In addition to a performance objective, a competing cost objective is introduced. Denoted f_2, this objective is chosen to be the number of layers in the unit cell:

$$\text{Minimize: } f_2 = n. \tag{29}$$

Pareto plots generated by the multiobjective genetic algorithm are shown in Fig. 6a. The run-time parameters of the genetic algorithm are given in Appendix (Table A1). The values of $n_{\max}=16$ and $l=30$ were used for the mixed and binary formulations, respectively, and for the mixed formulation, $1/l$ was taken as the minimum layer thickness. The values for $n_{\max}$ and l were chosen to allow a larger design freedom than the case reported in Hussein et al. (2002), which was based on the objective given by Eq. 28 and also had $\Omega^*=20$ as the target frequency. The optimal design in that

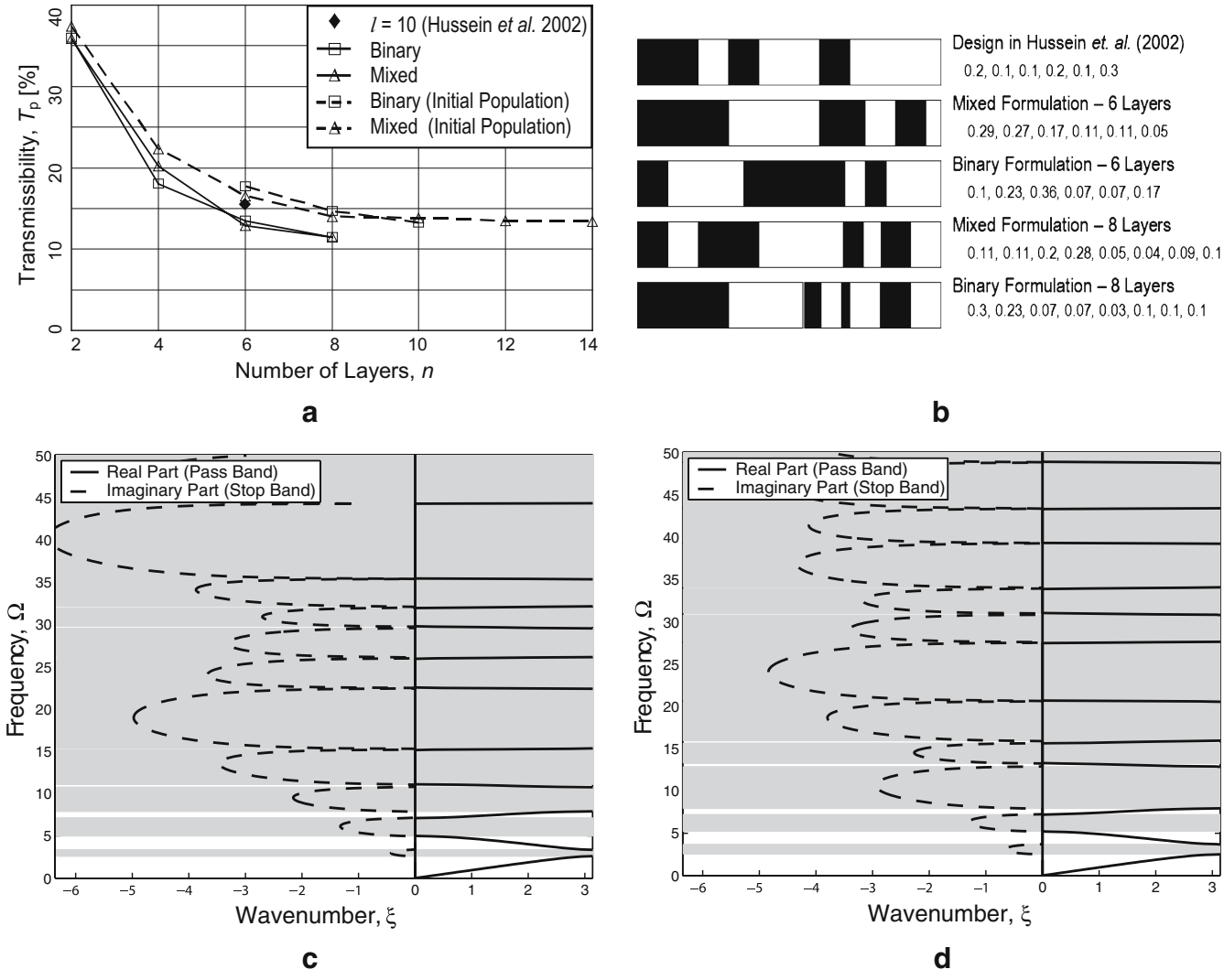

Fig. 7 Case II (minimization of transmissibility for flat load distribution spanning $0 \leq \Omega^* \leq 50$): **a** Pareto diagram ($l=30$ for both mixed and binary formulations), **b** selected unit cell designs from the Pareto front. Frequency spectrum for eight-layer design obtained by **c** the mixed formulation and **d** the binary formulation (stop bands *shaded in gray*)

paper (obtained by exhaustive enumeration following the binary formulation with $l=10$) is shown as a reference point in Fig. 6a, and its layout is shown in Fig. 6b. The number of layers of that design is $n=10$, and the imaginary value of the wave number at the specified frequency is $\xi_{\text{imag}}=-8.01$. It should be noted that $l=30$ makes an exhaustive search highly impractical since it would require 2^{28} ($\approx 2.7\times 10^8$) function evaluations[2].

The Pareto plots in Fig. 6a show that the multiobjective genetic algorithm found improved designs ($\xi_{\text{imag}}=-8.55$) using the same number of layers as in Hussein et al. (2002) as well as even better designs using 12 layers. No better designs were found by increasing the number of layers beyond 12. The unit-cell layouts of a selection of the best designs are shown in Fig. 6b. Note that these unit cells are not primitive; that is, they consist of subcells. This is due to the fact that an inherent length scale has been incorporated in the design objective through the specified target nondimensional frequency Ω^*. For maximum band-gap attenuation at that frequency, several of these subcells are required to form the optimal unit cell. Dispersion curves for two of the best designs (performance-wise) are presented in Fig. 6c and d. It should be noted for both plots that while the stopband is not centered around $\Omega^*=20$, the design maximizes $\left|\xi_{\text{imag}}\right|$ at that specified frequency. An objective to control the size of the band gap (while centralizing it around a specified frequency or around a minimized central frequency) could alternatively

[2] It can be shown that the size of the combinatorial search space is equal to 2^{l-2}.

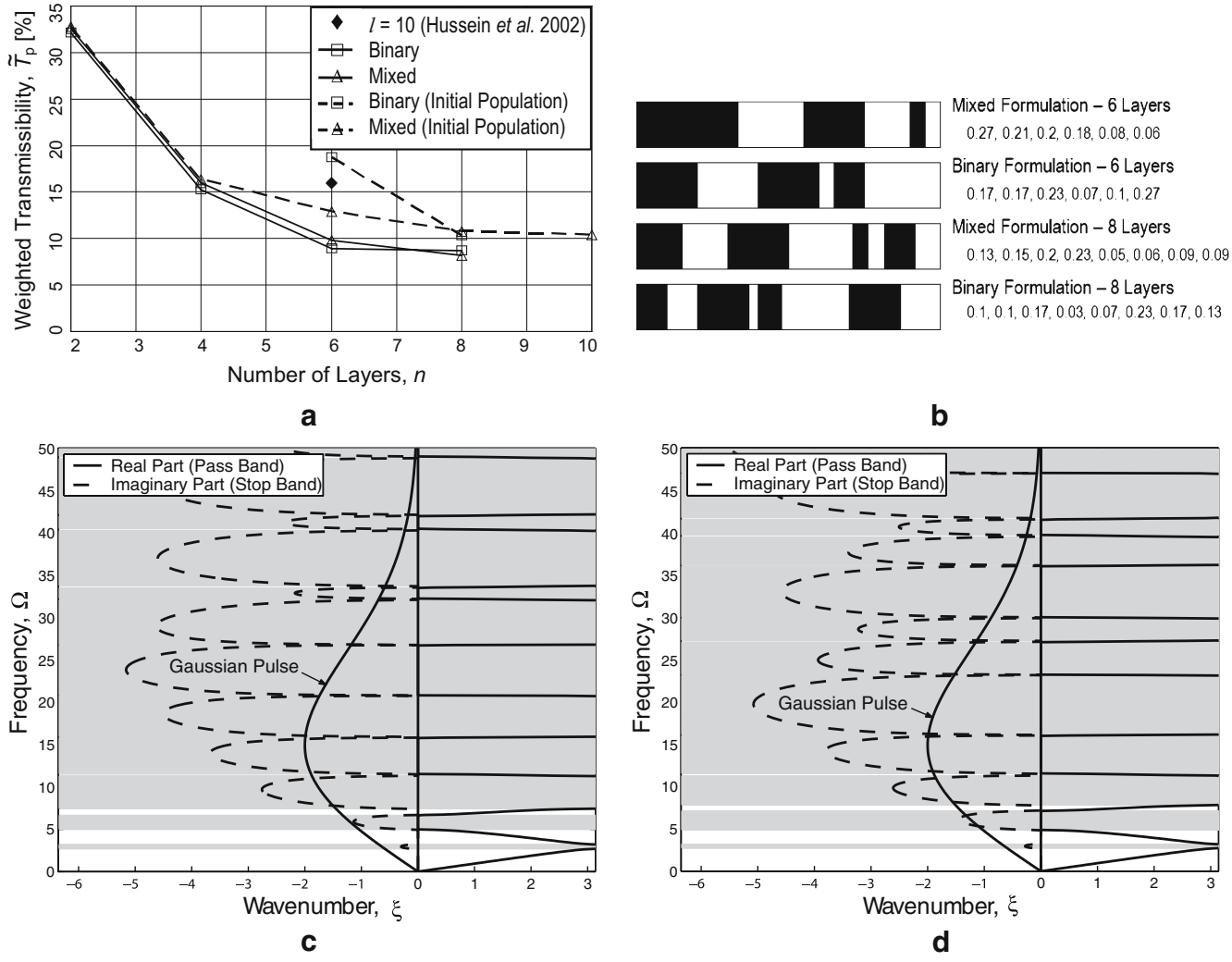

Fig. 8 Case II (minimization of transmissibility for Gaussian load distribution spanning $0 \leq \Omega^* \leq 50$): **a** Pareto diagram (l=30 for both binary and mixed formulations), **b** selected unit cell designs from the Pareto front. Frequency spectrum for eight-layer design obtained by **c** the mixed formulation and **d** the binary formulation (stop bands *shaded in gray*)

be considered following the same process; however, this is likely to be at the expense of maximizing $|\xi_{\text{imag}}|$.

4.2 Case II: maximization of the percentage of stopbands within a specified large frequency range for minimum transmissibility

The objective in this case study is to minimize the transmission of an incident general transient pulse. Transient pulses typically have broad frequency content, and in most practical cases, it may be impossible that a stopband can be synthesized with enough width to cover the whole frequency range of the pulse. For example, in case I, the maximum band-gap width achieved is $\Delta\Omega \approx 30$, while it may be desirable to suppress a pulse with a wider bandwidth. For this reason, an alternate performance measure, *transmissibility*, is taken as the performance objective f_1. In this study, transmissibility, denoted T_p, is defined as the percentage of the sum of frequency ranges where a passband exists to the total frequency range, $\Omega_{\min} \leq \Omega^* \leq \Omega_{\max}$, of the pulse that is to be isolated. This definition leads to the following statement:

$$\text{Minimize: } f_1 = T_p = 100 \times \frac{\int_{\Omega_{\min}}^{\Omega_{\max}} H(\xi_{\text{real}}(\Omega))\mathrm{d}\Omega}{\Omega_{\max} - \Omega_{\min}}, \quad (30)$$

where $H(\xi_{\text{real}}(\Omega))$ is a hard limit function defined as

$$H(\xi_{\text{real}}(\Omega)) = \begin{cases} 1 \text{ if } \xi_{\text{real}} > 0 \text{ (passband)} \\ 0 \text{ if } \xi_{\text{real}} = 0 \text{ (stopband)} \end{cases}. \quad (31)$$

The cost objective f_2 is defined in Eq. 29, as in case I. The relationship to the finite structure is again through the mapping $\Omega_{\min/\max} = \omega_{\min/\max}\, d \Big/ \sqrt{E_m/\rho_m}$, where $\omega_{\min/\max}$ denotes

the lower and upper limits of the actual frequency range of the shock load, respectively.

Consider first a case where the frequency content is constant over a range of $0 \leq \Omega^* \leq 50$ ($\Omega_{\min} = 0$ and $\Omega_{\max} = 50$). The mixed formulation with $n_{\max}$=16 and a=1/l, and the binary formulation with l=30, were implemented. The run-time parameter values for the genetic algorithm are the same as in case I and are given in Appendix (Table A1). The resulting Pareto plots are presented in Fig. 7a. The performance of the design reported by Hussein et al. (2002) (which employed an exhaustive search with l=10) is $T_{\rm p}$=16.3%, and the cost is n=6 layers. A data point for this result is included in Fig. 7a for comparison. The multiobjective genetic algorithm found superior designs ($T_{\rm p}$=12.9%) with n=6 and even better designs ($T_{\rm p}$=11.5%) for n=8. No better designs were found with more than eight layers. This observed layer saturation emanates from the limit on the minimum size of the layers below which dispersion in the medium will not occur. Note that for a given maximum temporal frequency limit, there is a corresponding minimum wavelength (maximum wave number) limit associated with the appropriate Brillouin zone. For dispersion to occur, the minimum wavelength in the scattered field should not significantly exceed the length scale of the layers. The unit-cell layouts of selected best designs are shown in Fig. 7b. The frequency spectra for the best performing designs (using both formulations) are shown in Fig. 7c and d. In practice, finite forms of these types of designs could be realized as mounting devices for shock isolation and as surface pads or wall partitions for sound isolation.

Consider now the more general case of a pulse with variable frequency content. The performance objective f_1 is modified by introducing a weighting function that takes into account the frequency distribution of the pulse. This way, a bias is introduced to give preference for the appearance of stopbands in regions in the spectrum where the frequency content of the pulse is high. For example, consider the problem of designing a periodic material that is to be tailored to isolate a double-Gaussian pulse of the form

$$g(t) = \mathrm{e}^{-a(t-b)^2} - \mathrm{e}^{-a(t-c)^2} \tag{32}$$

where a, b, and c are parameters. For $\hat{g}(\omega)$ [the Fourier transform of $g(t)$] to approximately span the frequency range $0 \leq \Omega^* \leq 50$, the parameters are chosen as follows:

$$a = 450, b = 0.25, c = 0.26. \tag{33}$$

The performance objective f_1 in this case involves the weighted transmissibility, $\tilde{T}_{\rm p}$:

$$\text{Minimize: } f_1 = \tilde{T}_{\rm p} = 100 \times \int_{\Omega_{\min}}^{\Omega_{\max}} G(\Omega) H(\xi_{\rm real}(\Omega)) \mathrm{d}\Omega, \tag{34}$$

Table 1 Target stopbands and target passbands for case III example

Target stopbands			
SB_1:	SB_2:		SB_3:
$10 < \Omega \leq 20$	$25 < \Omega \leq 35$		$40 < \Omega \leq 45$
Target passbands			
PB_1:	PB_2:	PB_3:	PB_4:
$0 < \Omega \leq 10$	$20 < \Omega \leq 25$	$35 < \Omega \leq 40$	$45 < \Omega \leq 50$

where $G(\Omega) = \alpha \hat{g}(\omega)$ and α is determined such that

$$\int_{\Omega_{\min}}^{\Omega_{\max}} G(\Omega) \mathrm{d}\Omega = 1. \tag{35}$$

The Pareto plots in Fig. 8a show the performances/costs of designs obtained via weighted optimization (using the mixed and binary formulations and same run-time parameters as above) for the frequency range of $0 \leq \Omega^* \leq 50$. Similar to the nonweighted case, no better designs were found with more than eight layers. However, with the weighted objective, the performance of the designs is observed to improve by about 3–4% across the Pareto front. Unit-cell designs with a weighted transmissibility as remarkably low as $\tilde{T}_{\rm p} = 8.2\%$ are realized. The unit-cell layouts of selected best designs are shown in Fig. 8b, and the frequency spectra of the best performing designs (using both formulations) are shown in Fig. 8c and d.

It should be noted that this novel approach of incorporating the frequency content of the excitation into the optimization scheme (to favorably bias the synthesis of the designed material's frequency band structure) is generally applicable to any arbitrary form of excitation.

4.2.1 Remarks

Cases I and II show that the multiobjective genetic algorithm could find better designs than the ones reported by Hussein et al. (2002)—this is because the optimization problems treated have been relaxed by allowing a larger design space. The mixed formulation is a relaxation of the binary formulation. However, the dependency of the size of **d** on n in the mixed formulation decreases the efficiency of the genetic algorithm, a phenomenon known as *epistasis* (Goldberg 1989). This is a likely reason why the binary formulation found better designs than the mixed formulation for most cases. The binary formulation has the advantages that the optimized layer thickness values require no truncation, and that the layer dimensions

Table 2 Target stopbands and target passbands for case III example

Target stopbands			
SB_1:	SB_2:	SB_3:	SB_4:
$0 < \Omega \leq 10$	$20 < \Omega \leq 25$	$35 < \Omega \leq 40$	$45 < \Omega \leq 50$
Target passbands			
PB_1:	PB_2:		PB_3:
$10 < \Omega \leq 20$	$25 < \Omega \leq 35$		$40 < \Omega \leq 45$

are multiples of a certain value and hence could be manufactured in standard sizes. On the other hand, for a fixed length binary string, an increase in the number of cell layers implies a loss of resolution because fewer bits are allocated per layer. From a practical perspective, the advantages of the binary formulation outweigh those of the mixed formulation especially since the results show that the maximum difference in performance in favor of the mixed formulation does not exceed 1%.

It is interesting to note that while the mixed and binary solutions corresponding to 6, and 8, layers in both Figs. 7 and 8 are very close in performance, their respective designs are notably different. These results demonstrate nonuniqueness and shed some light on the multimodality of the considered objectives. Note that the objectives involve a summation over a frequency range, and therefore the net sum (objective value) could be similar for different band structures and hence for different designs. In fact, this observation supports the assertion of the existence of numerous local optima, which, in turn, provides strong justification for the use of a heuristic evolutionary optimization technique such as NSGA-II.

4.3 Case III: creation of multiple stopbands/passbands at specified frequency ranges

In this case study, the objective is to impede wave propagation at multiple specific frequencies. A material designed with such characteristics could be used to form a structure that is required to isolate vibration under multiharmonic exci-

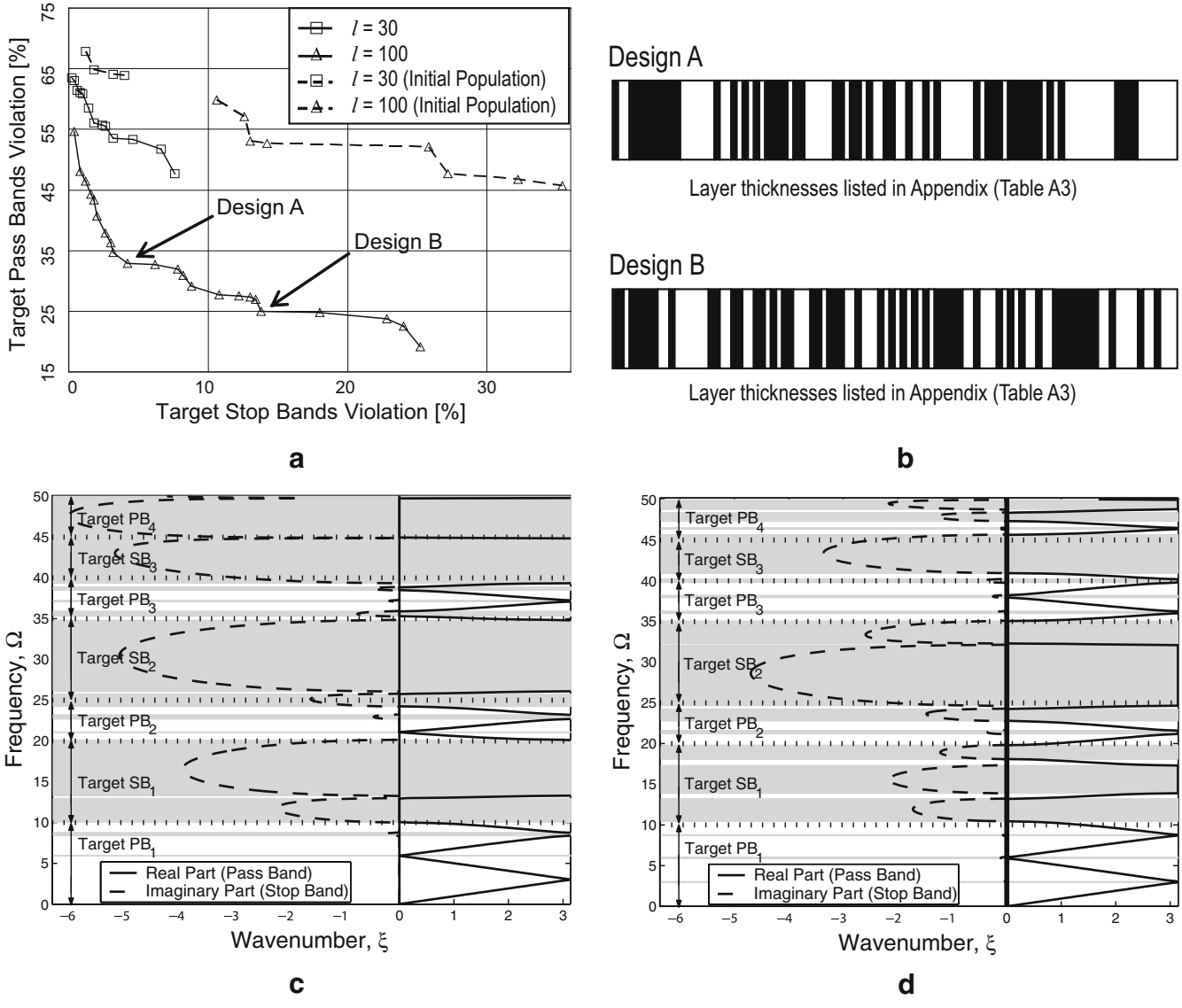

Fig. 9 Case III (creation of multiple bands as given in Table 1): **a** Pareto diagram (binary formulation), **b** selected unit cell designs from the Pareto front. Frequency spectrum for **c** design A and **d** design B (stop bands *shaded in gray*)

tation. Although a case II design may also be suitable for this application, it would not guarantee that the band gaps cover the various specific excitation frequencies. Furthermore, in some engineering applications, it might be desirable to have passbands lie adjacent to the target isolation frequency ranges (the target stopbands) to allow the excitation energy to pass through.

To achieve this design goal, two performance objectives are formulated, and for simplicity, no cost objective is considered. The first objective targets the achievement of attenuation at specified stopband frequency ranges, whereas the second targets the achievement of propagation at the complementary passband frequency ranges. More specifically, the first objective f_1 is to minimize the percentage "lack of creation" of desired stopbands (i.e., stopbands violation), and the second objective f_2, defined similarly, is to minimize the percentage "lack of creation" of desired passbands (i.e., passbands violation):

$$\text{Minimize: } f_1 = 100 \times \frac{\int_{\Omega_{\min}}^{\Omega_{\max}} G_{\mathrm{S}}(\Omega) H(\xi_{\mathrm{real}}(\Omega)) \mathrm{d}\Omega}{\int_{\Omega_{\min}}^{\Omega_{\max}} G_{\mathrm{S}}(\Omega) d\Omega}, \quad (36)$$

and

$$\text{Minimize: } f_2 = 100 \times \frac{\int_{\Omega_{\min}}^{\Omega_{\max}} G_{\mathrm{P}}(\Omega)(1 - H(\xi_{\mathrm{real}}(\Omega))) \mathrm{d}\Omega}{\int_{\Omega_{\min}}^{\Omega_{\max}} G_{\mathrm{P}}(\Omega) d\Omega}, \quad (37)$$

where $G_{\mathrm{S}}(\Omega)$ and $G_{\mathrm{P}}(\Omega)$ are the target stopband and passband weighing functions, respectively, and are defined as

$$G_{\mathrm{S}}(\Omega) = \begin{cases} 1 \text{ if } \Omega_{\min}^{\mathrm{SB}_i} \le \Omega \le \Omega_{\max}^{\mathrm{SB}_i}, i = 1, \ldots, \mathrm{SB}_{\max} \\ 0 \text{ otherwise} \end{cases}, \quad (38)$$

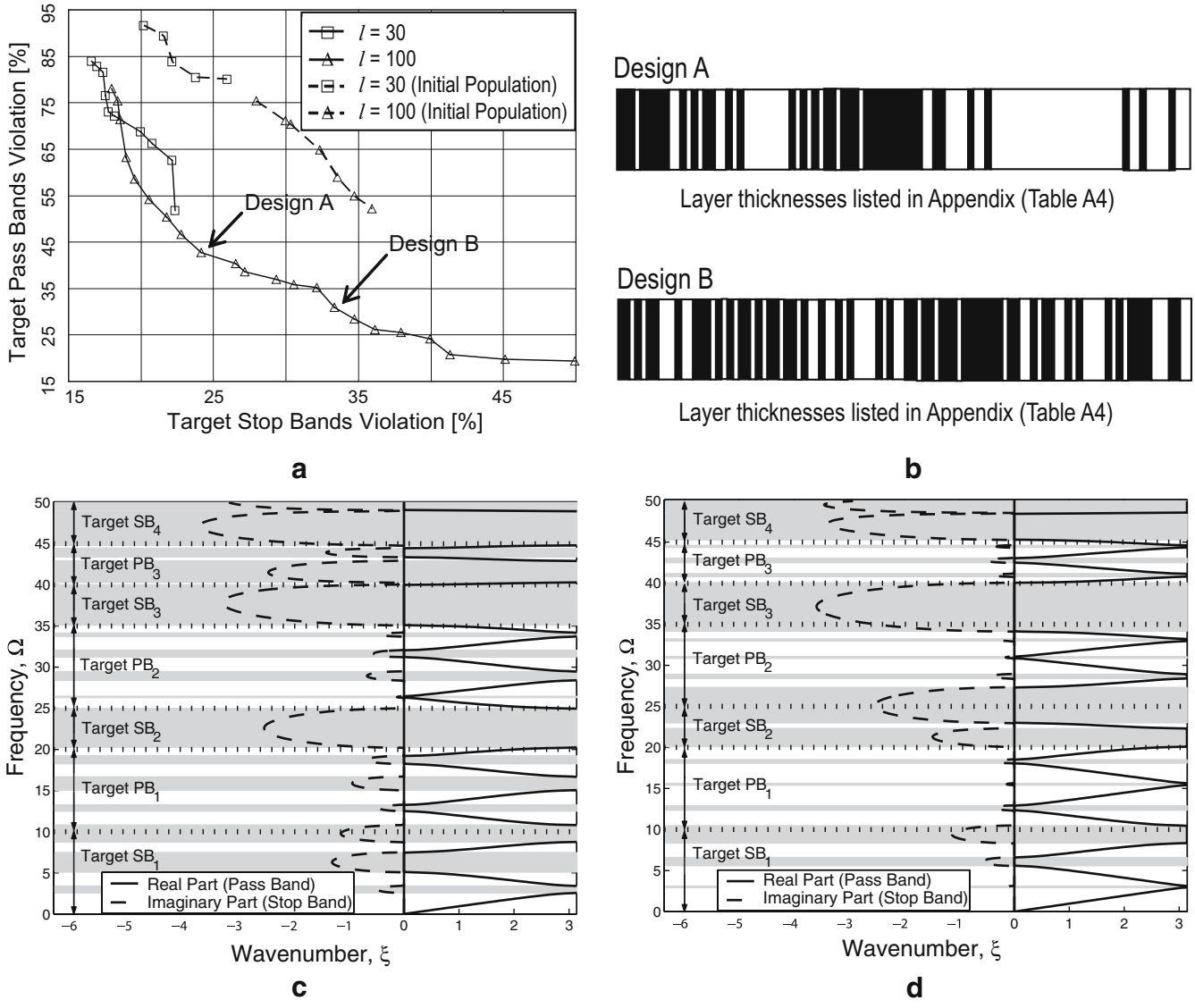

Fig. 10 Case III (creation of multiple bands as given in Table 2): **a** Pareto diagram (binary formulation), **b** selected unit cell designs from the Pareto front. Frequency spectrum for **c** design A and **d** design B (stop bands *shaded in gray*)

$$G_{\mathrm{P}}(\Omega) = \begin{cases} 1 \text{ if } \Omega_{\min}^{\mathrm{PB}_i} \le \Omega \le \Omega_{\max}^{\mathrm{PB}_i},\ i = 1, \ldots, \mathrm{PB}_{\max} \\ 0 \text{ otherwise} \end{cases} . \tag{39}$$

In Eqs. 38 and 39, the *i*th stopband and passband are denoted by SB_i and PB_i, respectively (enumeration starts with lowest frequency band). The number of the maximum stopband and passband considered is defined as $\mathrm{SB}_{\max}$ and $\mathrm{PB}_{\max}$, respectively, and the formula for relating the nondimensional and actual frequencies is $\Omega_{\min/\max}^{\mathrm{SB}_i/\mathrm{PB}_i} = \omega_{\min\,/\,\max}^{\mathrm{SB}_i/\mathrm{PB}_i} d \Big/ \sqrt{E_{\mathrm{m}}/\rho_{\mathrm{m}}}$, as previously noted. Note that the specific target frequency ranges could collectively cover a broadband if the multiharmonic excitation spans a wide frequency range.

As an example, consider the two sets of design parameters (criteria) given in Tables 1 and 2. The first set represents three desired stopbands and four desired passbands, all within the range $0 < \Omega \le 50$. The second set represents the "complement" of the first set with all the desired stopband ranges replaced with desired passband ranges and vice versa. Using the binary formulation, two Pareto plots are generated (for l=30 and l=100) and are shown in Figs. 9a and 10a, respectively. The run-time parameter values for the genetic algorithm in this case are given in Appendix (Table A2). Clearly, the difference in the design performances is significant between the l=30 and l=100 sets, especially for f_2 for both criterion sets. For the design parameters given in Table 1, f_2 at best is approximately 20% (violation), whereas the stopband objective, on the other hand, ranges from approximately 0.5 to 25% (violation). Similarly, for the design parameters given in Table 2, the passband objective at best is also approximately 20%, whereas f_1 ranges from approximately 17% to at least 50%. This shows that it is more difficult to design for passbands than it is to design for stopbands, when the design objectives encompass both target passbands and target stopbands. Numerous experimentation with different band targets should give further insight into this issue. The unit-cell layouts of two selected best designs for the first criterion set are shown in Fig. 9b (layer thickness values are given in Table A3), and their frequency spectra are presented in Fig. 9c and d. Also, layouts of two selected best designs for the second criterion set are shown in Fig. 10b (layer thickness values are given in Table A4), and their frequency spectra are presented in Fig. 10c and d. Because the design objectives encompass substantially more target frequency ranges compared to cases I and II, the resultant layer topologies are more complex.

5 Summary and conclusions

In this study, a multiobjective genetic algorithm was used for the design of periodic layered materials for desired frequency band structure (size and location of stopbands/passbands within the medium's frequency spectrum). The following three case studies were considered—(1) case I: maximizing wave attenuation capacity at a single specified frequency; (2) case II: maximizing the percentage of stopbands within a specified large frequency range, with and without a superimposed weight function to account for the frequency content of the pulse to be isolated; and (3) case III: synthesizing multiple stopbands/passbands at specified frequency ranges. The first and third cases apply to the problem of vibration isolation (or filtering) under single and multiple harmonic excitation, respectively, whereas the second case applies to the problems of shock and sound (or any general transient pulse) isolation.

Two formulations were developed, for each of cases I and II, namely, mixed-integer programming (mixed formulation) and zero–one integer programming (binary formulation). The formulations were implemented on example problems. The Pareto plots for both sets of results indicated that an increase in the number of cell layers improves the wave attenuation performance. Furthermore, better unit-cell designs were found compared to those previously reported (Hussein et al. 2002). The results also show that the relevant measure of wave attenuation saturated at approximately 12 layers for periodic materials designed to stop a time harmonic wave and approximately 8 layers for isolation of transient pulses spanning a wide frequency range. The saturation is attributed to the existence of limits on the ratio of wavelength to the minimum characteristic length scale in the unit cell, above which the medium is nondispersive. The designed unit cells in case I had an attenuation strength as high as $\left|\xi_{\mathrm{imag}}\right| \approx 8.3$, and in case II, a weighted transmissibility as low as $\tilde{T}_{\mathrm{p}} \approx 8\%$. In case III (implemented only using the binary formulation), it was shown that unit cells can be tailored to exhibit multiple stopbands/passbands at specified frequency ranges, but with less precision for targeted passbands.

The presented design approach suggests remarkable promise for generating periodic materials that could be used for forming bounded structures with advanced vibration, shock/sound isolation, or filtering characteristics. The results also motivate extending this approach to multidimensional structures, which is the topic of future research.

Appendix

Table A1 Run-time parameters of genetic algorithm used in cases I and II

	Mixed formulation	Binary formulation
Population size	120	100
Number of generations	80	100
Crossover probability (overall)	0.90	0.90
Crossover probability (number of layers gene)	0.05	implicit
Mutation probability	0.02	0.02
Number of runs	5	5

Table A2 Run-time parameters of genetic algorithm used in case III

	Binary, l=30	Binary, l=100
Population size	100	200
Number of generations	100	150
Crossover probability	0.90	0.90
Mutation probability	0.02	0.02
Number of runs	5	5

Table A3 Layer thicknesses for selected case III designs for objective given in Table 1

Layer number, j	d_j (10^{-2})	Layer number, j	d_j (10^{-2})	Layer number, j	d_j (10^{-2})	Layer number, j	d_j (10^{-2})
Design A							
1	1	12	1	23	2	34	3
2	2	13	4	24	2	35	1
3	9	14	1	25	1	36	5
4	6	15	2	26	2	37	1
5	1	16	5	27	1	38	1
6	2	17	2	28	1	39	1
7	1	18	1	29	1	40	1
8	1	19	2	30	1	41	9
9	1	20	1	31	6	42	4
10	1	21	1	32	1	43	1
11	1	22	2	33	1	44	6
Design B							
1	2	14	1	27	1	40	1
2	1	15	2	28	1	41	1
3	5	16	3	29	1	42	2
4	2	17	2	30	1	43	1
5	1	18	1	31	1	44	2
6	6	19	3	32	1	45	8
7	2	20	2	33	5	46	2
8	2	21	1	34	2	47	1
9	2	22	3	35	1	48	4
10	2	23	1	36	3	49	1
11	2	24	1	37	1	50	2
12	1	25	1	38	1	51	1
13	1	26	1	39	1	52	3

Table A4 Layer thicknesses for selected case III designs for objective given in Table 2

Layer number, j	d_j (10^{-2})	Layer number, j	d_j (10^{-2})	Layer number, j	d_j (10^{-2})	Layer number, j	d_j (10^{-2})
Design A							
1	3	11	1	21	2	31	1
2	1	12	1	22	1	32	23
3	5	13	1	23	3	33	1
4	2	14	8	24	1	34	2
5	1	15	1	25	10	35	1
6	1	16	1	26	2	36	4
7	1	17	1	27	2	37	1
8	1	18	1	28	4	38	3
9	2	19	1	29	1		
10	2	20	1	30	2		
Design B							
1	2	16	1	31	1	46	1
2	1	17	1	32	1	47	2
3	1	18	1	33	1	48	2
4	1	19	2	34	2	49	1
5	2	20	1	35	2	50	1
6	3	21	2	36	1	51	1
7	1	22	1	37	2	52	4
8	2	23	1	38	1	53	1
9	3	24	2	39	3	54	1
10	1	25	1	40	1	55	1
11	1	26	2	41	7	56	1
12	1	27	1	42	1	57	4
13	1	28	1	43	2	58	3
14	1	29	1	44	2	59	2
15	2	30	4	45	1	60	2

References

Burger M, Osher SJ, Yablonovitch E (2004) Inverse problem techniques for the design of photonic crystals. IEICE Trans Electron E87C:258–265

Cao WW, Qi WK (1995) Plane-wave propagation in finite 2–2-composites. J Appl Phys 78:4627–4632

Cox SJ, Dobson DC (1999) Maximizing band gaps in two dimensional photonic crystals. SIAM J Appl Math 59:2108–2120

Cox SJ, Dobson DC (2000) Band structure optimization of two-dimensional photonic crystals in *H*-polarization. J Comput Phys 158:214–224

Day NA, Zhu C, Kinra VK (1994) A study of dispersive wave propagation in periodic layered composites. Proc. Review of Progress in Quantitative Nondestructive Evaluation (held in Brunswick, Maine, 1993) vol. 13A. Plenum Press, New York, pp 243–250

Deb K (2001) Multi-objective optimization using evolutionary algorithms. Wiley, London

Deb K, Argawal S, Pratab A, Meyarivan T (2000) A fast elitist non-dominated sorting genetic algorithm for multi-objective optimization: NSGA-II. In: Lecture notes in computer science no. 1917, parallel problem solving from Nature VI Conference. Springer, Paris, France, pp 849–858

Esquivel-Sirvent R, Cocoletzi GH (1994) Band-structure for the propagation of elastic-waves in superlattices. J Acoust Soc Am 95:86–90

Floquet G (1883) Sur les Équations Différentielles Linéaries à Coefficients Périodiques. Ann Éc Norm 12:47–88

Goldberg D (1989) Genetic algorithms in search optimization and machine learning. Addison-Wesley Pub. Co., Reading, MA

Hussein MI (2004) Dynamics of banded materials and structures: analysis, design and computation in multiple scales. Ph.D. Thesis. University of Michigan, Ann Arbor, MI

Hussein MI, Hulbert GM, Scott RA (2002) Tailoring of wave propagation characteristics in periodic structures with multilayer unit cells. Proc. 17th American Society of Composites Technical Conference (held in West Lafayette, Indiana 2002), CD ROM, pp 1–9

Hussein MI, Hulbert GM, Scott RA (2003) Band-gap engineering of elastic wave guides using periodic materials. Proc. ASME International Mechanical Engineering Congress and R&D Expo (held in Washington, DC, 2003). ASME Publication, New York, pp 799–807

Hussein MI, Hamza K, Hulbert GM, Scott RA, Saitou K (2004a) Design of layered structures with desired dispersion properties using a multi-objective genetic algorithm. Proc. 8th Cairo University International Conference on Mechanical Design and Production (held in Cairo, Egypt, 2004), pp 41–50

Hussein MI, Hulbert GM, Scott RA (2004b) Effects of "finiteness" on wave propagation and vibration in elastic periodic structures. Proc. ASME International Mechanical Engineering Congress and R&D Expo (held in Anaheim, CA, 2004). ASME Publication, New York, pp 437–447

Hussein MI, Hulbert GM, Scott RA (2005) Dispersive elastodynamics of 1D banded materials and structures: analysis. J Sound Vib (in press)

Jensen JS (2003) Phononic band gaps and vibrations in one- and two-dimensional mass-spring structures. J Sound Vib 266:1053–1078

Kushwaha MS (1996) Classical band structure of periodic elastic composites. Int J Mod Phys B 10:977–1094

Michalewicz Z (1996) Genetic algorithms+data structures=evolution programs, 3rd edn. Springer, Berlin Heidelberg New York

Sigmund O, Jensen JS (2003) Systematic design of phononic band-gap materials and structures by topology optimization. Philos Trans R Soc Lond, A 361:1001–1019

Shen MR, Cao WW (2000) Acoustic bandgap formation in a periodic structure with multilayer unit cells. J Phys D Appl Phys 33:1150–1154

Thomson WT (1950) Transmission of elastic waves through a stratified solid medium. J Appl Phys 21:89–93